Magnetic Behaviour of Tetrakis[(2-diethylaminoethanolato)isocyanatocopper(II)], a Complex with an Antiferromagnetic Ground State; the Crystal and Molecular Structure of the Triclinic Modification†

Ludwig Schwabe and Wolfgang Haase *
Institut für Physikalische Chemie, Technische Hochschule Darmstadt, Petersenstrasse 20, 6100 Darmstadt, West Germany

The crystal and molecular structure and magnetic behaviour of [{Cu(NCO)(OCH$_2$CH$_2$NEt$_2$)}$_4$] (**B**) from benzene have been determined. The crystal structure determination was carried out by single-crystal *X*-ray diffraction methods and refined to $R = 0.066$ for 4 379 independent reflections: triclinic, space group $P\bar{1}$, with unit-cell dimensions $a = 13.478(3)$, $b = 12.873(3)$, $c = 11.542(3)$ Å, $\alpha = 84.020(5)$, $\beta = 80.263(5)$, and $\gamma = 86.863(5)$°. Each copper atom is five-co-ordinated by three oxygen and two nitrogen atoms. The magnetic susceptibility measured over the temperature range 5.0—302.5 K shows a maximum at 94 K and thus indicates that antiferromagnetic spin coupling is dominant. The magnetic behaviour can be explained on the basis of the isotropic Heisenberg–Dirac–van Vleck model. The results are compared with the structural and magnetic properties of the tetragonal form (**A**) of this complex. No phase transition between the two modifications could be found up to the melting point.

Merz and Haase[1] showed that the compound [{Cu(NCO)(OCH$_2$CH$_2$NEt$_2$)}$_4$] obtained by crystallization from methanol forms tetrameric molecules (**A**) of the cubane type having magnetic and structural properties characteristic of tetrameric copper(II) complexes of the transition type. These compounds are from the magnetic point of view characterized by the simultaneous presence of antiferromagnetic and ferromagnetic exchange effects of the same order of magnitude, whereas in the case of type I or II complexes the antiferromagnetic (type I) or the ferromagnetic interaction (type II) dominates. From the structural point of view a classification of the different types of tetrameric complexes can also be given.[2]

In this paper we report on a new tetrameric copper(II) complex of the transition type. By recrystallization from benzene, two modifications of the complex [{Cu(NCO)(OCH$_2$CH$_2$NEt$_2$)}$_4$] were obtained. The cell parameters of the tetragonal modification are the same as for (**A**). The properties of the triclinic form (**B**) will be discussed here.

A comparison of the structural and magnetic properties for different modifications of the same compound is of great interest for magnetostructural correlations. In our compounds the difference in magnetic parameters is caused only by the variation of the molecular geometry. Up to now this example seems to be the only tetrameric copper(II) complex, for which the crystal structures of the polymorphic forms have been determined. Other examples have been reported where the recrystallization leads to different molecular structures with incorporated solvent.[3–6]

Experimental

Preparation.—The preparation of complex (**A**) followed the procedure of Merz and Haase.[1] Dark green single crystals of complex (**B**) were obtained by recrystallization of (**A**) from a dilute solution of benzene. In case of a high concentration of benzene a tetragonal modification was obtained. The absence of benzene in the crystal was demonstrated by proton n.m.r. spectroscopy.

Crystallography.—*Crystal data.* C$_{28}$H$_{56}$Cu$_4$N$_8$O$_8$, $M = 886.96$, triclinic, $a = 13.478(3)$, $b = 12.873(3)$, $c = 11.542(3)$ Å, $\alpha = 84.020(5)$, $\beta = 80.263(5)$, $\gamma = 86.863(5)$°, $U = 1\,961.6$ Å^3 (by least-squares refinement of 48 strong reflections, $\lambda = 0.71069$ Å, measured at 299 K), space group $P\bar{1}$ (no. 2),[7] D_m (flotation) $= 1.48(3)$ g cm^{-3}, $Z = 2$, $D_c = 1.503$ g cm^{-3}. Dark green rhombic crystals: dimensions (distances to faces from centre) 0.095 (100,$\bar{1}$00) × 0.323 (001,00$\bar{1}$) × 0.323 (110,$\bar{1}\bar{1}$0) mm, μ(Mo-K_α) = 21.14 cm^{-1}, $F(000) = 904$.

Data collection and processing. STOE-STADI4 four-circle diffractometer, scan $\omega:\theta = 1:1$ in the range $3 \leqslant 2\theta \leqslant 45$°, graphite-monochromated Mo-K_α radiation. 6 447 Reflections measured, 4 889 unique, merging $R = 0.0223$ after absorption correction (maximum, minimum transmission factors = 0.6260 and 0.2550), giving 4 379 with $I > 3\sigma(I)$. Three strong reflections monitored every 50 reflections showed constant intensity.

Structure determination. The positions of the four copper and the four oxygen atoms within the Cu$_4$O$_4$ core were derived by direct methods. After some Fourier syntheses all non-hydrogen atoms were located ($R = 0.30$). Some least-squares cycles and anisotropic refinement of the thermal parameters led to $R = 0.077$. After geometrical positioning of the H atoms (C–H 1.08 Å) and final least-squares refinement cycles R converged at 0.066. The final Fourier difference map showed some peaks (< 0.6 e Å^{-3}) in the neighbourhood of the ethyl groups.

The obtained fractional co-ordinates and their standard deviations are listed in Table 1. All calculations were performed with the program SHELX 76[8] on the IBM 370/168 computer at the Technische Hochschule Darmstadt. The scattering factor of Cu^0, which is not stored in the program, was taken from ref. 9.

Magnetic Measurements.—The magnetic susceptibility of complex (**B**) was recorded on powder samples by the Faraday method at about 1 T in the temperature range 5.0—302.5 K. Experimental susceptibility data were corrected for the underlying diamagnetism (107×10^{-6} cm^3 per mol Cu

---

† *Supplementary data available* (No. SUP 56265, 4 pp.): thermal parameters, experimental and calculated susceptibilities. See Instructions for Authors, *J. Chem. Soc., Dalton Trans.* 1985, Issue 1, pp. xvii—xix. Structure factors are available from the editorial office.

Non-S.I. unit employed: B.M. ≈ 9.27×10^{-24} A m^2.

Table 1. Positional parameters of the non-hydrogen atoms of complex (**B**) with standard deviations in parentheses

Atom	*X*/*a*	*Y*/*b*	*Z*/*c*	Atom	*X*/*a*	*Y*/*b*	*Z*/*c*
Cu(1)	0.186 6(1)	0.819 2(1)	0.233 0(1)	C(122)	0.099 6(9)	1.065 1(8)	0.247 5(11)
Cu(2)	0.212 6(1)	0.588 3(1)	0.349 2(1)	C(131)	−0.012 7(8)	0.893 8(11)	0.162 7(11)
Cu(3)	0.409 7(1)	0.710 6(1)	0.237 7(1)	C(132)	−0.018 6(11)	0.803 5(11)	0.100 9(12)
Cu(4)	0.279 5(1)	0.783 4(1)	0.470 7(1)	C(22)	0.141 9(7)	0.469 8(7)	0.581 2(10)
O(11)	0.154 0(3)	0.747 5(3)	0.387 8(4)	C(211)	0.258 2(6)	0.615 9(6)	0.099 3(7)
O(12)	0.274 7(8)	0.969 2(7)	−0.100 7(7)	C(212)	0.261 2(7)	0.496 5(6)	0.134 0(8)
O(21)	0.264 9(3)	0.668 2(3)	0.203 3(4)	C(221)	0.211 9(8)	0.363 0(6)	0.298 2(10)
O(22)	0.132 3(5)	0.420 7(6)	0.671 2(8)	C(222)	0.310 5(8)	0.346 5(7)	0.335 5(10)
O(31)	0.335 5(3)	0.835 9(3)	0.283 7(4)	C(231)	0.087 0(6)	0.483 6(8)	0.232 7(11)
O(32)	0.567 3(7)	0.446 1(7)	0.115 5(6)	C(232)	0.052 0(9)	0.425 0(12)	0.140 7(14)
O(41)	0.333 4(3)	0.651 8(3)	0.416 4(4)	C(32)	0.522 2(6)	0.519 9(7)	0.159 5(7)
O(42)	0.246 0(6)	1.097 9(6)	0.503 9(10)	C(311)	0.390 3(5)	0.926 8(5)	0.249 8(7)
N(11)	0.040 4(4)	0.878 6(5)	0.265 3(6)	C(312)	0.488 0(9)	0.901 2(8)	0.207 8(15)
N(12)	0.222 4(5)	0.884 2(6)	0.076 2(7)	C(321)	0.616 8(10)	0.778 4(13)	0.211 8(17)
N(21)	0.191 7(4)	0.474 2(5)	0.244 9(7)	C(322)	0.644 5(8)	0.724 5(9)	0.303 8(10)
N(22)	0.148 8(6)	0.518 5(6)	0.495 0(7)	C(331)	0.552 9(16)	0.812 7(17)	0.049 5(12)
N(31)	0.526 5(4)	0.806 9(5)	0.170 7(6)	C(332)	0.550 9(14)	0.773 0(12)	−0.033 4(12)
N(32)	0.479 0(5)	0.582 7(5)	0.204 4(6)	C(42)	0.239 3(7)	0.999 8(9)	0.508 8(9)
N(41)	0.335 6(5)	0.735 8(5)	0.619 4(5)	C(411)	0.383 3(6)	0.588 1(6)	0.499 7(7)
N(42)	0.228 9(6)	0.916 7(5)	0.509 9(7)	C(412)	0.397 0(15)	0.647 9(13)	0.592 9(12)
C(12)	0.245 2(7)	0.926 5(7)	−0.011 0(8)	C(421)	0.264 6(11)	0.705 6(16)	0.720 5(12)
C(111)	0.053 2(5)	0.768 3(6)	0.445 1(6)	C(422)	0.173 2(9)	0.743 0(10)	0.753 4(13)
C(112)	−0.009 4(6)	0.802 0(7)	0.356 5(8)	C(431)	0.395 2(14)	0.805 3(12)	0.661 2(15)
C(121)	0.038 3(7)	0.985 3(7)	0.313 9(11)	C(432)	0.457 8(9)	0.875 8(9)	0.605 2(13)

estimated by Pascal's increment method). Magnetic moments were calculated using the formula $\mu = 2.828(\chi T)^{\frac{1}{2}}$.*

Thermodynamic Measurements.—The thermodynamic investigations were performed by differential scanning calorimetry (d.s.c.) with a Du Pont 990 thermoanalyzer in the temperature range 300—500 K with a heating rate of 5 K min.$^{-1}$

Results and Discussion

Molecular Structure.—A perspective view of the molecule (**B**) is given in Figure 1. The distances and angles within the Cu_4O_4 core and their mean values assuming C_2 and S_4 symmetry are listed in Table 2 together with data for (A). In Table 3 the distances and angles within the ligands are presented. The molecule possesses the point symmetry C_1, but it can be described approximately by point symmetry C_2 and nearly by S_4.

While the copper–copper distances in complex (A) are equal within the error, in (**B**) they are different. In agreement with the assumed C_2 symmetry in (**B**) between the pseudo-dimeric units, two pairs of copper–copper distances are equivalent and longer than those in (A). The distances within the dimeric units are shorter than in (A) (Table 2). The copper atoms are five-coordinate. Cu–O distances are of the types chelate bonded (normal Cu–O bond length), intra-pseudo-dimeric non-chelate bonded [elongated, but shorter than in (A)], and inter-pseudo-dimeric [longer than in (A)]. So from a structural point of view, (**B**) can be considered more similar to type I complexes than (A). The bridging oxygen atoms have distorted tetrahedral coordination with a mean angle of 108.8°. The amino-nitrogen atom shows also a tetrahedral arrangement.

The dihedral angle within the pseudo-dimeric units, defined as the angle between the two planes through two oxygen and one copper atom [Cu(1)–O(11)–O(21) and Cu(2)–O(11)–O(21) 9.81°, Cu(3)–O(31)–O(41) and Cu(4)–O(31)–O(41) 11.34°] is slightly less than in (A) (12.4°). The best planes of the two Cu_2O_2 four-membered rings of the pseudo-dimeric units are approximately parallel ($\alpha = 0.37°$). The isocyanate groups are elongated with a mean angle N(n2)–C(n2)–O(n2) (n = 1—4) of 176.6°.

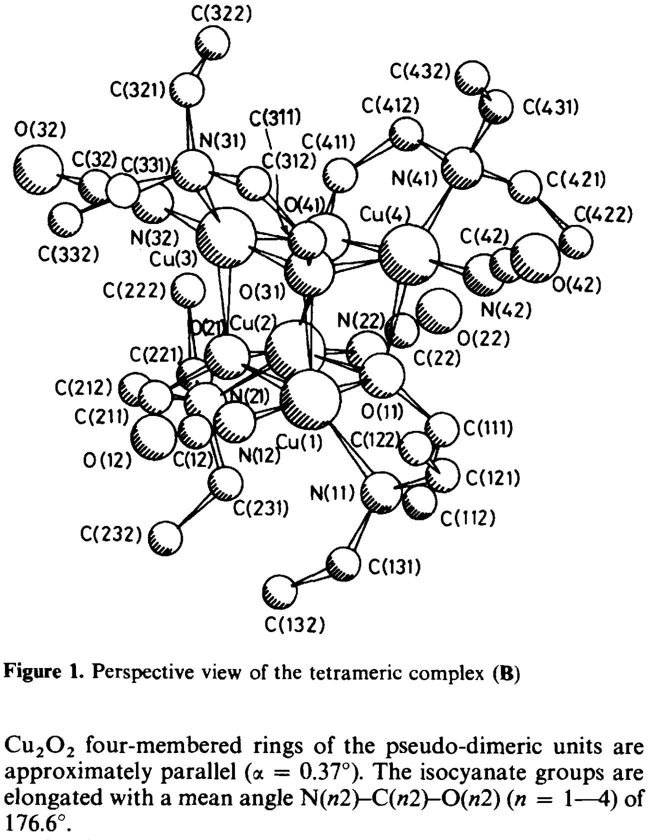

Figure 1. Perspective view of the tetrameric complex (**B**)

The thermal parameters of most atoms are greater than in complex (A), which might be caused by the smaller packing density in (**B**). Moreover, some ethyl groups have remarkably high thermal parameters corresponding to anomalously short bond lengths and angles. These distances and angles are marked by an asterisk in Table 3.

Crystal Packing.—The projection of the unit cell perpendicular to the (001) plane is shown in Figure 2. Two molecules in

---

* To convert into S.I. units, μ should be multiplied by $4\pi \times 10^{-6}$ and the magnetic moment is then given by the expression $\mu = 797.74\ (\chi T)^{\frac{1}{2}}$.

Table 2. Distances (Å) and angles (°) within the Cu_4O_4 core of complex (**B**) with standard deviations in parentheses

		Symmetry-equivalent mean values		For complex
		C_2	S_4	(**A**)
(*a*) Cu–Cu				
Cu(1)–Cu(2)	3.158(1)	3.158(1)		
Cu(3)–Cu(4)	3.153(1)	3.153(1)	3.156(3)	3.194(1)
Cu(1)–Cu(3)	3.254(1)			
Cu(2)–Cu(4)	3.240(1)	3.247(9)		
Cu(1)–Cu(4)	3.186(1)			
Cu(2)–Cu(3)	3.174(1)	3.180(9)	3.213(39)	3.194(1)
(*b*) Cu–O, (*i*) chelate bonded				
Cu(1)–O(11)	1.917(4)			
Cu(2)–O(21)	1.925(4)	1.921(6)		
Cu(3)–O(31)	1.926(4)			
Cu(4)–O(41)	1.930(4)	1.928(3)	1.925(5)	1.936(6)
(*ii*) Within the pseudo-dimers, non-chelate bonded				
Cu(1)–O(21)	2.192(4)			
Cu(2)–O(11)	2.217(4)	2.205(18)		
Cu(3)–O(41)	2.219(4)			
Cu(4)–O(31)	2.211(4)	2.215(12)	2.210(12)	2.243(6)
(*iii*) Between the pseudo-dimers				
Cu(1)–O(31)	2.211(4)			
Cu(2)–O(41)	2.151(5)	2.181(42)		
Cu(3)–O(21)	2.166(5)			
Cu(4)–O(11)	2.172(5)	2.169(5)	2.175(26)	2.113(6)
Cu(1)–O(11)–Cu(2)	99.4(2)			
Cu(1)–O(21)–Cu(2)	100.0(2)	99.7(4)		
Cu(3)–O(31)–Cu(4)	99.1(2)			
Cu(3)–O(41)–Cu(4)	98.7(2)	98.9(3)	99.3(5)	99.4(2)
Cu(1)–O(11)–Cu(4)	102.2(2)			
Cu(2)–O(21)–Cu(3)	101.6(2)	101.9(4)		
Cu(1)–O(31)–Cu(3)	103.5(2)			
Cu(2)–O(41)–Cu(4)	105.0(2)	104.3(9)	103.1(15)	104.0(2)
Cu(1)–O(21)–Cu(3)	96.6(2)			
Cu(2)–O(11)–Cu(4)	95.2(2)	95.9(9)		
Cu(1)–O(31)–Cu(4)	92.2(2)			
Cu(2)–O(41)–Cu(3)	93.1(2)	92.7(6)	94.3(20)	94.2(2)

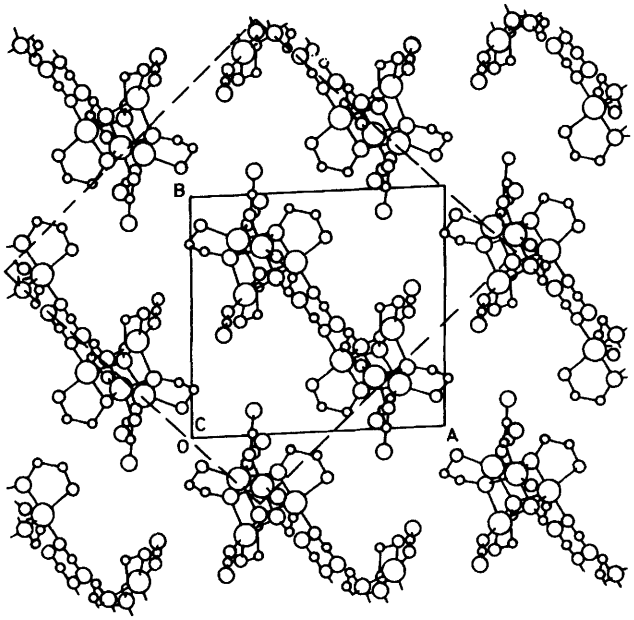

Figure 2. Projection of the unit cell of complex (**B**) perpendicular to the (001) plane

Table 3. Other distances (Å) and angles (°) within the molecule with standard deviations in parentheses

	$n = 1$	2	3	4
Cu(*n*)–N(*n*1)	2.061(5)	2.053(7)	2.053(6)	2.015(6)
O(*n*1)–C(*n*11)	1.431(4)	1.457(9)	1.404(8)	1.430(9)
C(*n*11)–C(*n*12)	1.448(12)	1.551(11)	1.360(13)*	1.427(18)
N(*n*1)–C(*n*12)	1.465(10)	1.464(10)	1.376(13)*	1.394(18)*
N(*n*1)–C(*n*21)	1.534(12)	1.526(10)	1.396(17)*	1.413(15)
C(*n*21)–C(*n*22)	1.429(14)	1.464(16)	1.304(22)*	1.308(19)*
N(*n*1)–C(*n*31)	1.476(15)	1.446(11)	1.379(15)*	1.406(20)
C(*n*31)–C(*n*32)	1.438(21)	1.514(21)	1.136(23)*	1.315(20)
Cu(*n*)–N(*n*2)	1.909(7)	1.902(8)	1.890(6)	1.882(7)
N(*n*2)–C(*n*2)	1.097(11)	1.113(13)	1.094(11)	1.084(14)
C(*n*2)–O(*n*2)	1.139(11)	1.150(13)	1.209(12)	1.266(14)
O(*n*1)–Cu(*n*)–N(*n*1)	84.3(2)	85.5(2)	85.7(2)	85.8(2)
Cu(*n*)–O(*n*1)–C(*n*11)	114.1(4)	113.3(4)	113.4(4)	113.7(4)
O(*n*1)–C(*n*11)–C(*n*12)	109.2(6)	108.3(6)	110.1(6)	109.6(8)
C(*n*11)–C(*n*12)–N(*n*1)	111.8(7)	108.6(6)	127.2(9)	121.3(14)
Cu(*n*)–N(*n*1)–C(*n*12)	103.3(4)	105.5(5)	101.6(6)	105.2(7)
Cu(*n*)–N(*n*1)–C(*n*21)	109.9(5)	114.2(6)	114.8(7)	116.3(7)
Cu(*n*)–N(*n*1)–C(*n*31)	115.9(6)	105.7(6)	114.2(10)	117.8(7)
C(*n*12)–N(*n*1)–C(*n*21)	110.0(7)	110.1(6)	111.1(11)	107.1(11)
C(*n*12)–N(*n*1)–C(*n*31)	111.1(7)	114.1(8)	111.5(12)	106.7(11)
C(*n*21)–N(*n*1)–C(*n*31)	106.7(8)	107.4(7)	103.9(12)	103.0(11)
N(*n*1)–C(*n*21)–C(*n*22)	118.6(9)	113.9(7)	137.0(13)*	129.5(15)*
N(*n*1)–C(*n*31)–C(*n*32)	116.6(11)	118.5(8)	145.8(20)*	131.4(15)*
O(*n*1)–Cu(*n*)–N(*n*2)	177.1(3)	174.2(3)	175.6(2)	175.0(3)
N(*n*1)–Cu(*n*)–N(*n*2)	97.8(3)	96.3(3)	97.3(3)	98.5(3)
Cu(*n*)–N(*n*2)–C(*n*2)	175.6(9)	158.5(8)	163.6(7)	150.0(7)
N(*n*2)–C(*n*2)–O(*n*2)	176.0(11)	178.3(10)	176.0(9)	175.9(11)

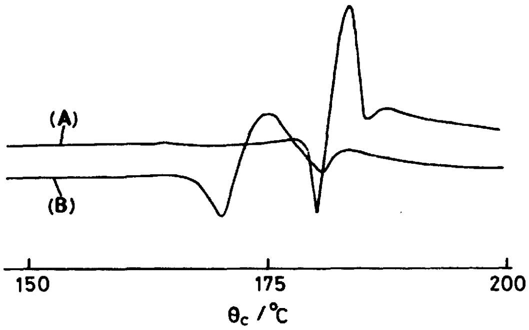

Figure 3. Measurements of the melting points of the compounds (**A**) and (**B**)

the unit cell are oriented with the pseudo-C_2 axis near the square diagonal.

In complex (**A**) four molecules are located along the [100] or [010] axis alternating in $z = 0$ or 0.5 with the $\bar{4}$ axis parallel to the [001] axis.[1] This kind of packing can also be detected in (**B**) by transforming the triclinic cell into a tetragonal cell assuming a higher symmetry (dotted axis in Figure 2). Assuming $\alpha = \beta = \gamma = 90°$, the transformation is given by $c' = c$, $a' = b' = (a^2 + b^2)^{\frac{1}{2}}$, so the square diagonals in the plane (001) of complex (**B**) become the a and b axis in (**A**).

Comparing the volumes of the unit cells for the two modifications, the greater value for (**B**) (3 923 Å^3 for two unit cells) than for (**A**) (3 798 Å^3) at the same temperature indicates a closer packing in (**A**).

Thermodynamic Properties.—No phase transition between both modifications could be detected up to the melting point. The melting point of complex (**B**) is 11.4 K lower than that of (**A**) (449.3 and 437.9 K) (see Figure 3). This can be interpreted in accordance with the greater volume of the unit cell in (**B**). In

Table 4. Magnetic parameters of complex (**B**) for different symmetries and comparison with those of (**A**) (ref. 1)

Symmetry	g	x	J_{12}/cm^{-1}	J_{34}/cm^{-1}	J_{13}/cm^{-1}	J_{14}/cm^{-1}	Δ
(**A**) S_4	2.19	0.014	−21.4(5)		+12.3(1)		0.4895
(**B**) S_4	2.196	0.062	−58.3(5)		+17.4(5)		1.3921
C_{2v}	2.196	0.052	−74.9(5)	−42.5(5)	+17.4(5)		0.581
C_2	2.225	0.049	−76.2(5)	−42.2(5)	+20.4(5)	+11.7(5)	0.570

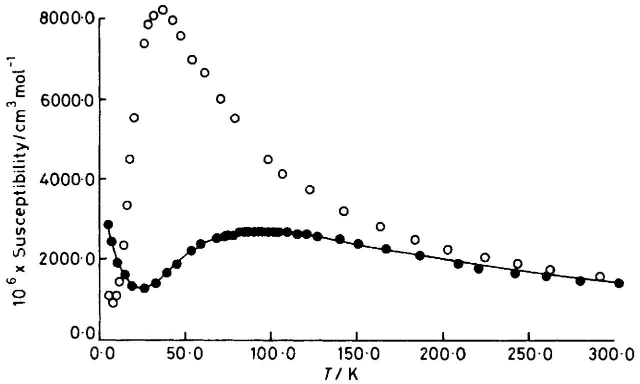

Figure 4. Temperature dependence of the magnetic susceptibility of complexes (**A**)[1] (○) and (**B**) (●). Experimental points for (**B**) are compared with the calculated values (full line)

d.s.c. analysis one endothermic (destruction of the lattice) and two exothermic (decomposition of the molecules) effects were observed. It is impossible to calculate the enthalpies of melting because the exo- and endo-thermic effects cannot be separated.

Magnetic Properties.—The temperature dependence of the magnetic susceptibility of complex (**B**) in the range 5.0—302.5 K is shown in Figure 4. The susceptibility data show a maximum at 94 K, and below this temperature down to 25 K the susceptibility decreases. At lower temperatures the susceptibility increases again, due to paramagnetic impurities. The magnetic moment is 0.33 B.M. at 5.0 K and rises to 1.85 B.M. at 302.5 K. The maximum of the susceptibility of complex (**A**) is situated at 34 K, whereas at room temperature it exhibits the same paramagnetic behaviour as does (**B**) (Figure 4).

The magnetic properties of the spin-coupled copper(II) complexes can be explained in terms of the isotropic Heisenberg–Dirac–van Vleck model. The exchange Hamiltonian is given by equation (1). Figure 5 shows the principal arrangement of the copper atoms in the molecule. In case of S_4 symmetry as realized in complex (**A**) two different J values result. In (**B**) the C_1 symmetry leads to six different J values; assuming C_2 symmetry four different exchange integrals are necessary, and for C_{2v} symmetry three exchange integrals will be obtained. The Hamiltonians for the three symmetry cases of interest are as in equations (2)—(4). The formulae for the magnetic susceptibility are well known[10] and will not be repeated here.

$$\mathscr{H} = -2\sum_{i,j} J_{ij}S_iS_j \tag{1}$$

$$S_4\colon \mathscr{H} = -2J_{12}(S_1S_2 + S_3S_4) - 2J_{13}(S_1S_3 + S_1S_4 + S_2S_3 + S_2S_4) \tag{2}$$

$$C_{2v}\colon \mathscr{H} = -2J_{12}S_1S_2 - 2J_{34}S_3S_4 - 2J_{13}(S_1S_3 + S_1S_4 + S_2S_3 + S_2S_4) \tag{3}$$

$$C_2\colon \mathscr{H} = -2J_{12}S_1S_2 - 2J_{34}S_3S_4 - 2J_{13}(S_1S_3 + S_2S_4) - 2J_{14}(S_1S_4 + S_2S_3) \tag{4}$$

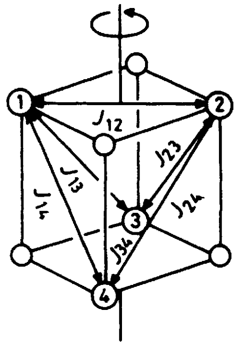

Figure 5. Principal structure of the Cu_4O_4 core showing the exchange integrals

The total paramagnetic susceptibility can be expressed as in equation (5) where χ_{para} is the paramagnetic susceptibility caused by impurities and x is their mol fraction. The temperature-independent paramagnetism (t.i.p.), N_α, was fixed at 60 × 10^{-6} cm^3 per mol Cu. The exchange integrals were evaluated by fitting equation (5) to the experimental susceptibility data using the least-squares SIMPLEX routine of Olsson.[11] The criterion for ending the fitting was the minimum of expression (6). The susceptibility data below 15 K were omitted from the fitting procedure because in this region the main part of the susceptibility originates in the monomeric impurity. The agreement between the experimental and calculated values is shown in Figure 4. The magnetic parameters of complexes (**B**) and (**A**) are presented in Table 4.

$$\chi_{calc.} = (1 - x)\chi_{tetramer} + x\chi_{para} + N_\alpha \tag{5}$$

$$\Delta = \Sigma(\chi_{calc.} - \chi_{obs.}) \tag{6}$$

We now make some general remarks on the fitting procedure. The procedure leads to one set of magnetic parameters only for molecules with high symmetry and $S = 0$ ground state. In case of low symmetry more than one set of parameters can be obtained. The same problem is found for compounds with ferromagnetic ground states.[12–14] To solve this problem the calculations must be performed assuming a higher-symmetry model in the first step. In the following steps the symmetry is reduced. For complex (**B**) the fitting procedure ended with C_2 symmetry. This reflects that the number of antiferromagnetic exchange integrals remains constant on reducing the symmetry to C_1 and the shape of the susceptibility function is mainly determined by the antiferromagnetic exchange integrals.

Magnetostructural Correlations.—The magnetic behaviour of the two modifications (**A**) and (**B**) is in principle the same, *i.e.* the simultaneous presence of antiferro- and ferro-magnetic interactions of the same order of magnitude. This is typical for tetrameric cubane-like copper(II) complexes of the transition type.[1] However, the susceptibility data of (**A**) and (**B**) are quite different (Table 4).

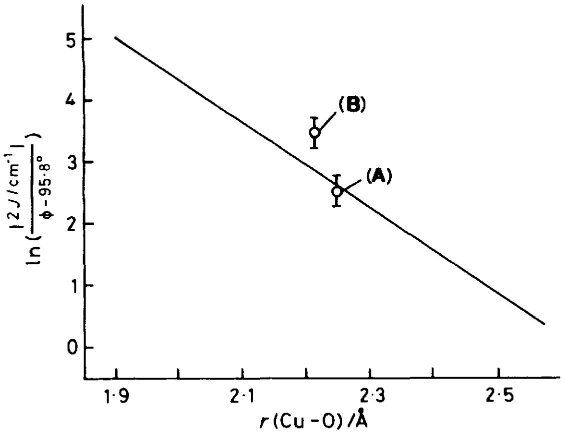

Figure 6. Correlation between the antiferromagnetic exchange integral and the intradimer Cu–O distance and the bridging angle[15] showing corresponding values for complexes (**A**) and (**B**)

To explain this difference we would like to compare the exchange integrals with the structural properties of the molecules. In case of the type I complexes and alkoxo-bridged dimers a correlation between the antiferromagnetic exchange integral and the related Cu–O–Cu bridging angle was described previously,[15] and for type II complexes a linear correlation between the ferromagnetic exchange integral and the interdimer Cu–O distance was demonstrated for some copper(II) complexes with ferromagnetic ground states.[10] Both correlations cannot be applied to transition-type complexes. Merz[10] developed a correlation between the antiferromagnetic exchange integral and two structural parameters, namely the Cu–O–Cu angle, φ, and the non-chelate bonded Cu–O distance, r, within the pseudo-dimeric unit [equation (7)]. Figure 6 shows

$$\ln[2J(\varphi,r)/(\varphi - 95.8)] = -ar + \text{constant} \qquad (7)$$

the straight line given by Merz[10] and the rather good agreement for modification (**A**). The value for (**B**) is slightly higher than the expected one.

The interpretation in the case of S_4 symmetry (Table 4) can be given in the usual way. The antiferromagnetic exchange integral characterizes the coupling within the two pseudo-dimeric units whereas the ferromagnetic one corresponds to the coupling between them. Thus, the ratio of $J_{\text{ferro}}/J_{\text{antiferro}}$ seems to be characteristic for each compound: 0.30 for (**B**) and 0.57 for (**A**). This confirms from a magnetic point of view the fact that (**B**) is more similar to type I complexes than is (**A**), as mentioned above. Further correlations assuming S_4 symmetry cannot be given because the mean values of distances and angles and their statistical deviations do not allow this. So we tried to correlate the exchange integrals with the structural parameters pertaining to C_2 symmetry.

Taking into account each individual distance and angle, we correlated the stronger antiferromagnetic exchange integral J_{12} to the pseudo-dimeric unit 1 [Cu(1)–O(11)–Cu(2)–O(21)]. This corresponds to the fact that the Cu–O–Cu angles are greater and the Cu–O distances shorter than in the dimeric unit 2 [Cu(3)–O(31)–Cu(4)–O(41)]. Both effects lead to a stronger antiferromagnetic coupling. Moreover we supposed that the main part of the exchange pathway in the dimeric unit 1 takes place in that oxygen bridge having the greatest angle and the shortest Cu–O distance [Cu(1)–O(21)–Cu(2)].

Acknowledgements

We thank the Deutsche Forschungsgemeinschaft for support and Dr. H. Paulus for data collection.

References

1 L. Merz and W. Haase, *J. Chem. Soc., Dalton Trans.*, 1978, 1594.
2 R. Mergehenn and W. Haase, *Acta Crystallogr., Sect. B*, 1977, **33**, 1877.
3 R. Mergehenn, L. Merz, and W. Haase, *J. Chem. Soc., Dalton Trans.*, 1980, 1703.
4 J. A. Bertrand and J. A. Kelley, *Inorg. Chim. Acta*, 1972, **6**, 248.
5 R. Mergehenn, L. Merz, W. Haase, and R. Allman, *Acta Crystallogr., Sect. B*, 1976, **32**, 505.
6 L. Schwabe and W. Haase, to be published.
7 'International Tables for *X*-Ray Crystallography,' 2nd edn., Kynoch Press, Birmingham, 1965, vol. 1.
8 SHELX 76, Program for Crystal Structure Determination, G. M. Sheldrick, Cambridge, 1976.
9 D. T. Cromer and J. B. Mann, *Acta Crystallogr., Sect. A*, 1968, **24**, 321.
10 L. Merz, Dissertation, Technische Hochschule Darmstadt, 1980.
11 D. M. Olsson, *J. Qual. Technol.*, 1974, **6**, 53.
12 J-P. Laurent, J-J. Bonnet, F. Nepveu, H. Astheimer, L. Walz, and W. Haase, *J. Chem. Soc., Dalton Trans.*, 1982, 2433.
13 H. Astheimer, F. Nepveu, L. Walz, and W. Haase, *J. Chem. Soc., Dalton Trans.*, 1985, 315.
14 J. Comarmond, P. Plueré, J-M. Lehn, Y. Agnus, R. Louis, R. Weiss, O. Kahn, and I. Morgenstern-Badarau, *J. Am. Chem. Soc.*, 1982, **104**, 6330.
15 L. Merz and W. Haase, *J. Chem. Soc., Dalton Trans.*, 1980, 875.

Received 19*th November* 1984; *Paper* 4/1960